Macromolecular Rapid Communications
www.mrc-journal.de

Transparent and Self-Healing Elastomers for Reconfigurable 3D Materials

Tiwa Yimyai, Abdon Pena-Francesch, and Daniel Crespy**

Transparent soft materials are widely used in applications ranging from packaging to flexible displays, wearable devices, and optical lenses. Nevertheless, soft materials are susceptible to mechanical damage, leading to functional failure and premature disposal. Herein, a transparent self-healing elastomer that is able to repair the polymer network via exchange reactions of dynamic disulfide bonds is introduced. Due to its self-healing ability, the mechanical properties of the elastomer can be recovered as well as its transparency after multiple cycles of abrasion and healing. The self-healing polymer is fabricated into 3D structures by folding or modular origami assembly of planar self-healing polymer sheets. The 3D polymer objects are employed as storage containers of solid and liquid substances, reactors for photopolymerization, and cuvettes for optical measurements (exhibiting superior properties to those of commercial cuvettes). These dynamic polymers show outstanding mechanical, optical, and recycling properties that could potentially be further adapted in adaptive smart packaging, reconfigurable materials, optical devices, and recycling of elastomers.

1. Introduction

Transparent soft materials have been extensively implemented on several applications in optics,[1] photovoltaics,[2–4] biomedical devices,[5,6] actuators,[7–9] and sensors,[10,11] where transparency of materials is a requirement of the applications in terms of light transmission, aesthetics, or see-through displays. The softness enables the materials to be flexible and compliant, however, it also makes them vulnerable to mechanical damage (scratches, cracks, punctures, abrasion, or cutting) and repeated physical stress. These damages consequently lead to unsatisfactory performance (loss of transparency due to light scattering) or loss of functionality, which eventually leads to a premature disposal.

Self-healing soft materials offer a promising solution to overcome the loss of functionality caused by mechanical damage by recovering the functions and properties of materials in many applications, such as electrical sensors,[12,13] thermal sensors,[14–16] or soft actuators[17,18] Self-healing materials have been developed following the two main approaches of intrinsic (designing molecular structure of the materials to contain dynamic reversible covalent or noncovalent bonds) and extrinsic systems (loading external healing agents into the matrix of materials).[19–21] Interestingly, intrinsic self-healing mechanisms are not only able to repair their mechanical, electrical, and optical properties but also enable the reconfiguration, reprocessing, and recycling of materials. For example, reprocessability and recyclability of self-healing materials containing aromatic disulfide bridges,[22] hydrogen–imine bonds,[23] reversible boronic ester bonds,[24] and urethane–hindered urea bonds[25] have been achieved upon thermal compression molding, which activated the mobility of polymer chains, enabling both physical chain diffusion and reversible formation/scission of dynamic bonds in the polymer network to recover their properties. Recently, efforts have been devoted to develop reconfigurable systems of diverse 3D shapes using self-healing polymeric materials via swelling by solvent[26] and transesterification reactions[27] in polymer networks. Shape-fixing could be also obtained by reversible deforming a self-healing polymer through thermal expansion/contraction by activation with infrared light[28] or through shape memory effect in self-healable thermosets.[25,29] Therefore, shape-fixing/reconfiguration of polymers with dynamic bonds can open new fabrication routes via the transformation of 2D into 3D structures, with applications in electronic devices,[30,31] packaging,[32,33] robotics,[34] and medical devices.[35–37] However, many self-healing polymers display low mechanical properties (post-healing ultimate tensile strain < 25%),[27,28] and contain colored additives (graphene or carbon nanotubes),[28,29] which limits their applications, especially for

T. Yimyai
Department of Chemical and Bimolecular Engineering
School of Energy Science and Engineering
Vidyasirimedhi Institute of Science and Technology (VISTEC)
Rayong 21210, Thailand
T. Yimyai, D. Crespy
Department of Materials Science and Engineering
School of Molecular Science and Engineering
Vidyasirimedhi Institute of Science and Technology (VISTEC)
Rayong 21210, Thailand
E-mail: crespy@mpip-mainz.mpg.de
A. Pena-Francesch
Department of Materials Science and Engineering
Macromolecular Science and Engineering, Robotics Institute
University of Michigan
Ann Arbor, MI 48109, USA
E-mail: abdon@umich.edu
The ORCID identification number(s) for the author(s) of this article can be found under https://doi.org/10.1002/marc.202200554

DOI: 10.1002/marc.202200554

materials requiring a combination of robustness, flexibility, and transparency. Thus, an intrinsic self-healing polymer that integrates both outstanding optical and mechanical properties would be a promising material to overcome the issues in optics and display applications.

Intrinsic self-healing polymers containing disulfide bonds exhibited excellent healing efficiency at moderate temperature (25–80 °C) due to low bond dissociation energy (60 kcal mol^{-1}) of disulfide metathesis reactions.[38–42] Most self-healing polymers containing disulfide bonds are yellowish and less transparent,[22,38–40,43,44] which limits their applications, especially for optical devices and displays. Herein, we introduced a self-healing polyurethane-based polymer containing dynamic disulfide bonds (PU-SH), which was prepared by a facile synthesis of polyaddition. The PU-SH polymer was colorless and highly transparent (high light transmittance), and provided recovery of mechanical and optical properties upon many cycles of damage and healing. The PU-SH polymers could be fabricated into 3D shapes via origami assembly methods of folding and modular reconfigurations to obtain 3D structures with seamlessly healed joints. We demonstrated temporary and permanent 3D shape-fixing of PU-SH polymers by taking advantage of its viscoelasticity and dynamic exchange reactions of disulfide bonds. The features of PU-SH offer 3D fabrication of structures and materials for optical applications that require self-healability and transparency as well as for packaging applications that can store liquid and solid materials. Then, we further demonstrate the 3D self-healing objects as containers for storing chemicals, reactors for photopolymerization, as well as cuvettes for optical measurements of dynamic light scattering (DLS) and ultraviolet-visible (UV–vis) spectroscopy (showing a performance equivalent to commercial quartz cuvettes).

2. Results and Discussion

A self-healing polymer (PU-SH) was synthesized via polyaddition of polytetrahydrofuran (PTHF) and dicyclohexylmethane 4,4'-diisocyanate (HMDI) to obtain a prepolymer and consequently reacted with 2-hydroxyethyl disulfide (HEDS) as a chain extender (**Figure 1**a). An equivalent non-self-healing polymer (PU) was prepared following the same procedure but used 1,6-hexanediol (HDO) as a chain extender instead. The chemical structures of PU-SH and PU polymers were confirmed by ^{1}H nuclear magnetic resonance (^{1}H-NMR) spectroscopy. As shown in Figure S1a,b in the Supporting Information, the signals of both PU-SH and PU around 3.36 and 1.57 ppm were attributed to aliphatic methylene protons of –O–CH_2– and –CH_2–CH_2–, respectively, and the characteristic peaks around 0.82–1.22, 1.91, and 3.47 ppm were assigned to alicyclic methylene protons of backbone in polymer chains. The characteristic peak at around 2.90 ppm corresponded to methylene protons of –CH_2–S– in PU-SH, which was absent for PU, indicating that PU-SH contained disulfide bonds, but PU did not. Functional groups in PU-SH and PU chemical structures were investigated by Fourier transform infrared (FTIR) and Raman spectroscopy. The FTIR spectra displayed characteristic peaks of PU-SH and PU, which included N–H stretching, CH_2 symmetric stretching, CH_2 antisymmetric stretching, hydrogen bond (H-bond) C=O urethane amide I, H-bond C–N stretching + N–H amide II bending, free –N stretching + N–H amide II bending, C–H wagging in CH_2, C–N stretching + N–H amide III bending, and C–O–C stretching at wavenumbers of 3323, 2931, 2855, 1700, 1532, 1448, 1369, 1229, and 1111 cm^{-1}, respectively (Figure 1b). The disulfide bonds in PU-SH were confirmed by Raman spectra (Figure 1c) with C–S stretching and S–S stretching at Raman shift of 641 and 510 cm^{-1}, respectively.

The self-healing properties of disulfide bonds in the molecular structure were verified by healing scratches of PU-SH and PU films at 70 °C for 30 min. The scratch (width ≈ 10 μm) on non-self-healing polymer (PU) remained after one healing cycle whereas the scratch on self-healing polymer (PU-SH) was visibly repaired (**Figure 2**a), demonstrating that PU-SH was able to self-heal at 70 °C while PU was not. To quantify the self-healing efficiency of the polymers, we performed tensile tests of pristine and healed PU-SH compared with non-self-healing polymer (PU) as a control sample (Figure 2b). The specimens with dog-bone shape (thickness = 0.2 ± 0.1 mm) were cut into two pieces and reconnected again, followed by healing at 70 °C for 24 h to obtain healed specimens. The average tensile strength (σ_{avg}) of pristine PU and PU-SH was 14.6 ± 1.2 and 8.1 ± 1.1 MPa, respectively with the corresponding average ultimate tensile strain (ϵ_{avg}) of 496% ± 31% and 625% ± 57%, respectively. A self-healing efficiency (ratio of tensile strength of healed samples to pristine samples) was calculated to compare the mechanical properties of the healed polymers. The healed PU displayed σ_{avg} of 1.9 ± 0.2 MPa and ϵ_{avg} of 92% ± 15%, which was much lower than that of pristine PU and resulted in a self-healing efficiency of 13%. On the contrary, the σ_{avg} and ϵ_{avg} of healed PU-SH were 8.0 ± 0.8 MPa and 596% ± 63%, which resulted in a self-healing efficiency of 98%. Therefore, the PU-SH polymer that exhibited better self-healing efficiency than PU, implying that disulfide bonds in the system of PU-SH promoted the self-healing beyond molecular chain diffusion.

We performed frequency-dependent rheological measurements at different temperatures from 10 to 90 °C to investigate the lifetime of the dynamic bonds in self-healing polyurethane polymer (PU-SH) and non-self-healing polymer (PU) polymers. Theoretically, crossover points between storage modulus (G') and loss modulus (G'') in a certain frequency (ω) at specific temperature is correlated to supramolecular bond lifetime ($1/\omega$) of self-healing polymers.[41,45,46] At higher temperature, exchange reactions of dynamic bonds were faster which enabled a greater self-healing. As shown in Figure 2c and Figure S2 in the Supporting Information, crossover points between G' and G'' of PU-SH and PU gradually shifted to higher frequency with increasing temperature, indicating that the dynamic exchange reactions in this polymer system were temperature dependent. At a healing temperature of 70 °C, the crossover points between G' and G'' of PU-SH appeared at ≈0.2 rad s^{-1}, which were not observed for PU. This clearly indicates that disulfide bonds play a central role in the healing process.

Taking advantage of the dynamic bonds, 3D objects were prepared with the PU-SH self-healing polyurethane elastomer. The healing property relied on the disulfide bond exchange reaction, taking place upon heating the elastomer.[41,42] The fabrication of 3D structures was performed by folding or assembling 2D planar self-healing polymer sheets with various shapes as well as by hierarchical assembly of 3D structures (**Figure 3**). First, open and

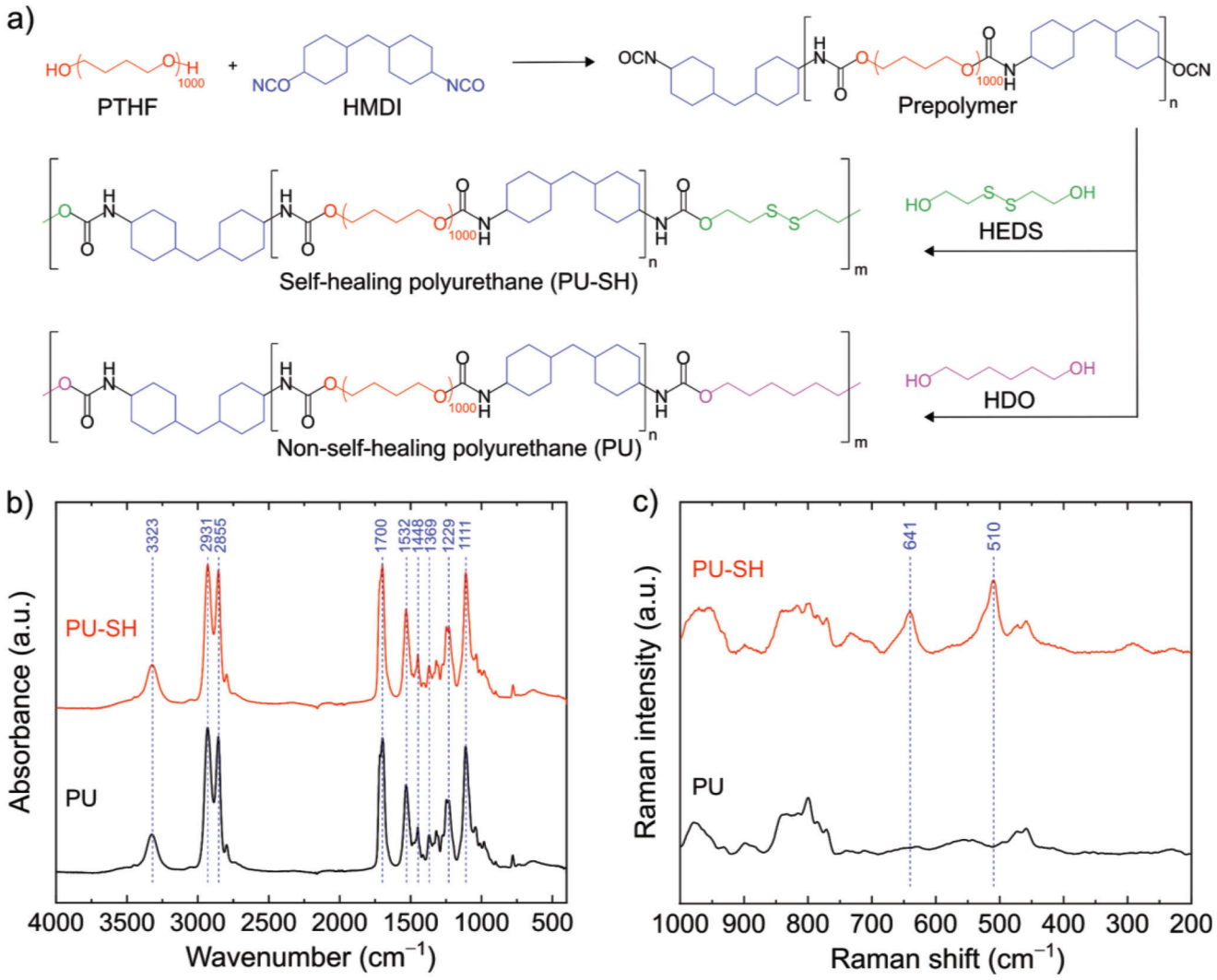

Figure 1. a) Synthetic routes for the preparation of self-healing polymer (PU-SH) and non-self-healing polymer (PU). b) Fourier Transform Infrared (FTIR) and c) Raman spectra of PU-SH and PU.

closed hollow cubes were fabricated by folding a 2D planar sheet (Figure 3a and Figure S3a, Supporting Information). The cubes were then covered with a folded PVC hollow closed cube mold to maintain its shape upon heating. After cooling, the hollow cube was retrieved by peeling the PVC outer layers. 3D objects could be also produced by assembling 2D polymer sheets (Figure 3b). Herein, we took advantage of the self-healing property of the elastomer to join the planar sheets. A closed hollow cube was assembled by joining six square planar sheets, which were then covered with PVC and followed by heating. A closed hollow cylinder was also assembled by joining one rectangular and two circular sheets (Figure S3b, Supporting Information), followed by heating. Moreover, hierarchical 3D objects could be assembled from modular 3D objects (Figure 3c). For example, closed hollow rectangular prisms were fabricated from the assembly of two open hollow cubes, followed by sealing of their edge.

Due to the self-healing ability of the material, these 3D structures can be potentially recycled to form other 3D structures. Therefore, the stability of self-healing polymer (PU-SH) after shape programming was investigated by quantifying the viscoelasticity of material after several cycles of shape-fixing. The shape-programming was conducted through a cycle of thermal treatment by heating PU-SH film (thickness = 0.30 ± 0.02 mm) at 70 °C for 24 h, and then cooling down to 25 °C. After three cycles of thermal treatment, the storage modulus (G') and loss modulus of (G'') of thermal treated PU-SH were comparable to pristine PU-SH (Figure S4a, Supporting Information). The results implied that the residual energy in PU-SH after several cycles of thermal change did not change significantly and that PU-SH maintained its stability after shape-fixing. We also examined viscoelastic behavior of the PU-SH polymer after several cycles of deformation. Circular 2D sheets were folded along their diameters at an angle of 90 ° and heated at 70 °C. The sheets were peeled off and flattened to yield circular planar sheets. The pristine circular sheet as well as the circular sheets recovered after several cycles were subjected to dynamic mechanical analysis (DMA) under oscillation strain sweep at 25 °C (Figure S4b, Supporting Information). The storage modulus (G') at linear viscoelastic region

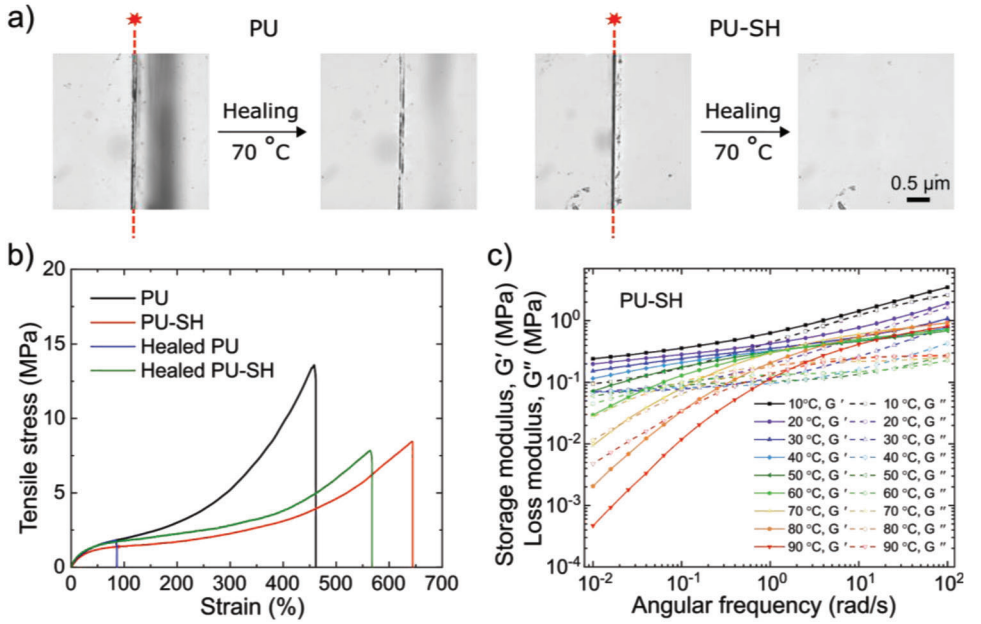

Figure 2. a) Optical microscopy images of scratched self-healing polymer (PU-SH) and non-self-healing polymer (PU) films before and after healing at 70 °C for 30 min. b) Tensile stress–strain curves of pristine and healed samples for PU and PU-SH. The healed samples were obtained by healing at 70 °C for 24 h. c) Storage modulus (G') and loss modulus (G'') as a function of frequency sweep at different sweeping temperature for PU-SH.

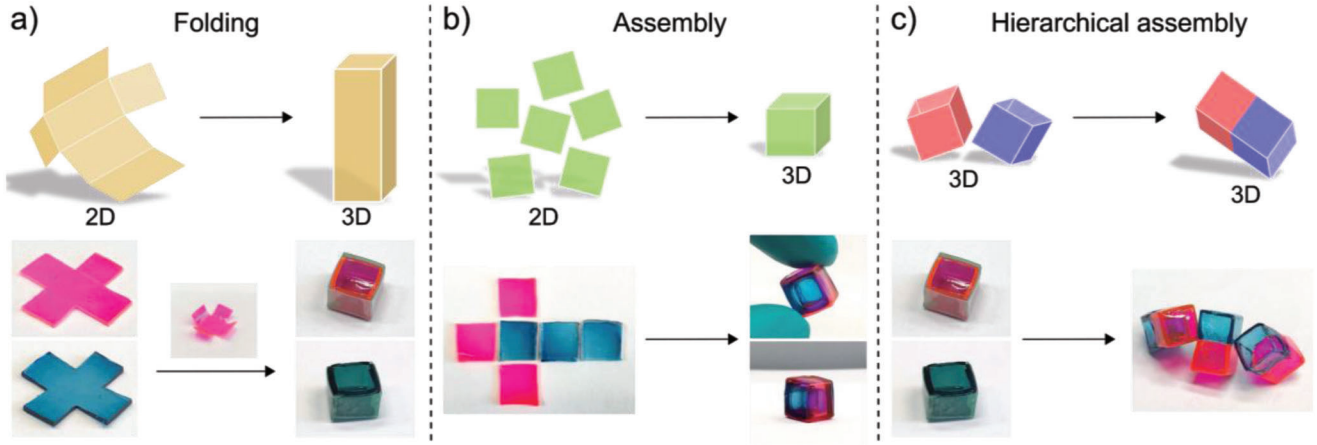

Figure 3. Conceptual scheme and photographs for shape programming of self-healing polymer sheets using a) folding of 2D shapes, b) assembly of 2D shapes to create 3D shapes, and c) hierarchical assembly of 3D shapes.

(a strain of 0.1%) of pristine and after cycles of deformation was not significantly different (≈0.10–0.11 MPa) as shown in (Figure S4c, Supporting Information), implying that the viscoelastic properties of the PU-SH polymer did not change after being deformed several times. G' of the self-healing polymer (PU-SH) was larger than for self-healing poly(urethane-urea)[47] ($G' = 0.2$ MPa) and thermoplastic polyurethanes[48,49] ($G' = 0.01$–0.015 MPa) at an oscillatory strain of 0.1% at 25 °C. Objects with this polymer could be reconfigured several times without loss of viscoelastic properties.

The PU-SH self-healing polymer exhibited high transparency, with a 92.8% transmittance in the 380–780 nm range of visible wavelength. Quartz glass and polystyrene (PS) displayed a transparency of 93.3% and 87.6% respectively (Figure S5, Supporting Information), with a measured transmittance spectra similar to previous reports in the literature.[50–52] Considering that quartz and PS are commonly used in optics and are used as consumables (like transparent containers such as cuvettes), self-healing PU-SH can potentially be a more durable alternative with equivalent optical properties. Furthermore, the surface of conventional cuvettes (quartz glass or PS) can be accidentally marked with scratches and abrasions, which can cause scattering of the light, making them unreliable for accurate measurements and hence requiring replacing of the cuvettes, which presents opportunities for self-healing and transparent materials. To test the feasibility, a PU-SH cuvette was fabricated by folding the corresponding 2D sheet into open rectangular prisms (Figure S6, Supporting Information), and the optical properties of the PU-SH and PS under

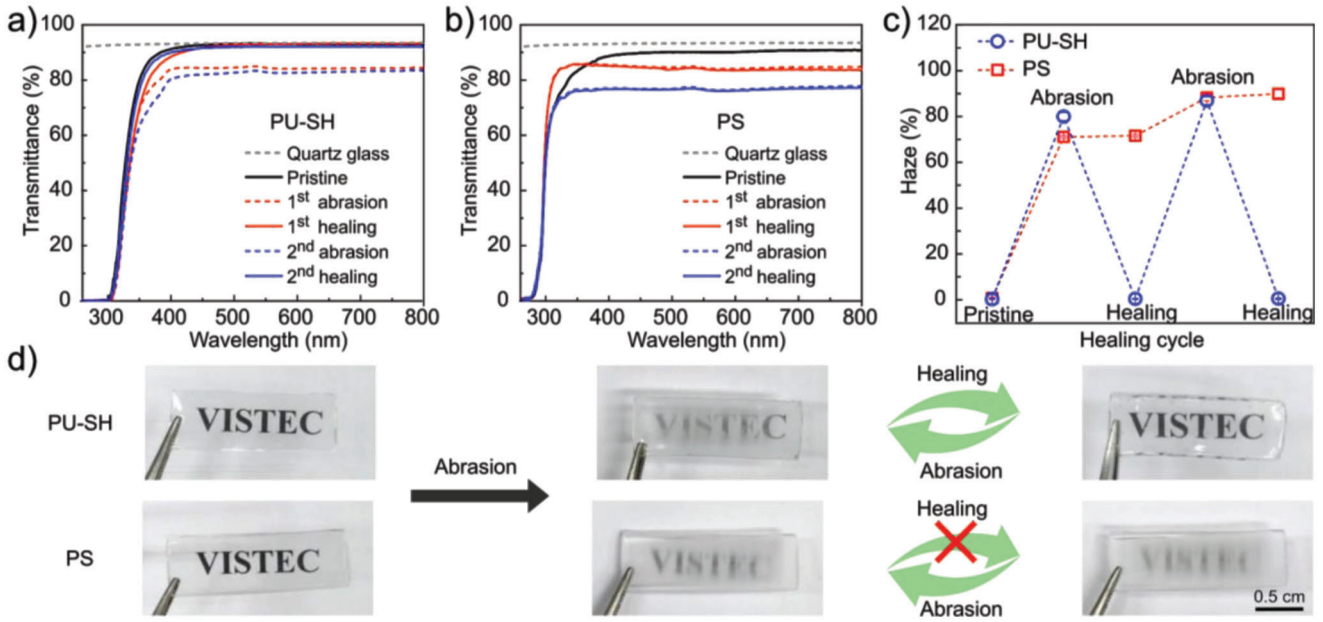

Figure 4. Ultraviolet–visible (UV–vis) light transmittance (T_2) spectra of pristine and abraded samples for a) a self-healing polymer (PU-SH) substrate (thickness = 0.78 ± 0.02 mm) and b) a polystyrene (PS) substrate (thickness = 1.0 mm). c) Average haze values over 380–780 nm of PU-SH and PS substrates after abrading with an abrasive paper and followed by healing at 70 °C. d) Photographs showing a reversible and irreversible change of haze appearance for PU-SH and PS after 40 cycles of abrasion and healing.

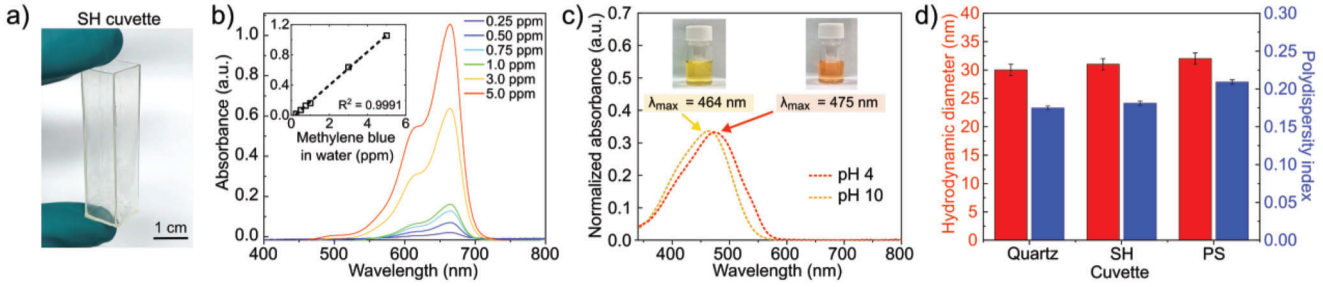

Figure 5. a) A self-healing plastic cuvette (SH cuvette) used for ultraviolet–visible (UV–vis) absorption and dynamic light scattering (DLS) measurements. b) Ultraviolet–visible (UV–vis) absorption spectra of methylene blue aqueous solution with various concentrations. The inset plot shows the linear relationship between UV–vis absorbance at λ_{max} = 664 nm and concentration of methylene blue aqueous solutions. c) UV–vis absorption spectra of methyl orange aqueous solutions at pH 4 and 10. d) Average hydrodynamic diameters (D_h) and polydispersity index (PDI) of silica nanoparticles measured using different types of cuvettes.

a treatment of abrasion and healing were analyzed. After abrasion, the intensity of transmitted light (T_2) by PU-SH and PS substrates decreased while the intensity of scattered light (T_4) increased (**Figure 4**a,b and Figure S7a,b, Supporting Information). The appearance of the substrates surfaces was compared by estimating their haze values (Figure 4c,d). The haze values of pristine PU-SH and PS substrates was 0.3% ± 0.1% and 0.8% ± 0.2%. After abrasion, the haze value of PU-SH increased to 80.0% ± 1.8% and 86.9% ± 1.7% for the first and second abrasion cycles, respectively. The haze values of PU-SH surfaces returned closely to the original transparency after healing (0.5% ± 0.2% and 0.6% ± 0.3% for the first and second healing, respectively). On the other hand, the haze value of abraded PS substrate was 71.6% ± 0.5% and remained as 71.6% ± 0.5% after being subjected to a healing cycle at 70 °C. The haze value of abraded PS substrate increased to 88.2% ± 1.4% when it was further abraded for 40 cycles, while the high transparency and low haze for PU-SH was recovered. This suggests that PU-SH can potentially be used as a self-healing and transparent materials platform for durable optical devices to robustly handle liquids, rough manipulation, and recover its properties after scratch, abrasion, or other types of mechanical damage.

To demonstrate a practical application of SH cuvettes (**Figure 5**a), we tested their performance and compared it to that of standard cuvettes in UV–vis spectroscopy and DLS measurements. First, we quantified the concentration of dyes in aqueous solutions, using methylene blue as a model dye. Calibration curves displaying absorbance against concentrations were created for solutions measured in the SH cuvette (Figure 5b), and as a control experiment, the calibration curve was also created for samples measured in the quartz cuvette (Figure S8, Supporting Information). Then, two solutions with specified amounts of methylene

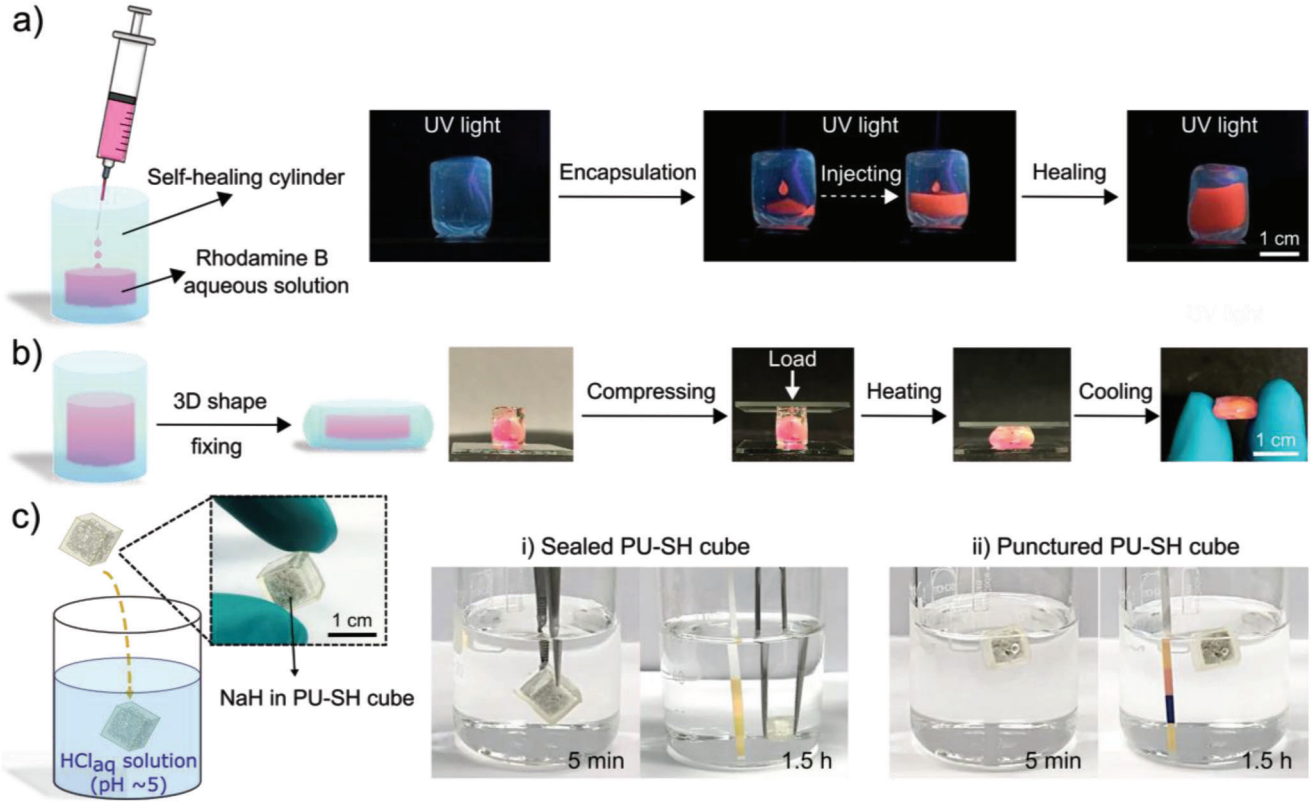

Figure 6. a) Sealing of a cylindrical recipient of self-healing polymer containing an aqueous solution of Rhodamine B. A closed hollow cylinder (left) was filled with the dye solution by puncturing the upper face of the cylinder with a needle to inject the dye solution (middle), followed by healing the punctured surface at 70 °C for 24 h (right). b) 3D shape fixing of a self-healing polymer cylinder containing an aqueous solution of Rhodamine B by mechanical compression at 70 °C. c,i) Sealed and ii) punctured self-healing hollow polymer cubes containing sodium hydride (NaH) were immersed in a slightly acidic aqueous solution (pH ≈ 5) for 5 min. After 1.5 h of immersion, the pH indicator strip (McolorpHast, Merck) in the aqueous medium for the sealed cube displayed different shades of yellow colors, indicating a constant pH ≈ 5 of the medium whereas the pH indicator strip turned to yellow, orange, and dark blue colors for the punctured cube, indicating pH ≈ 10.

blue in water (0.56 and 2.40 ppm) were prepared and analyzed in the quartz and SH cuvettes. The measured concentrations were 0.57 ± 0.01 ppm for both types of cuvettes for the lower concentration, and 2.40 ± 0.02 and 2.39 ± 0.03 ppm were measured in the self-healing and quartz cuvettes respectively for the upper concentration (2.40 ppm).

To further validate the applications of PU-SH in optical measurements, the SH cuvettes were used to measure the UV absorbance of methyl orange. Methyl orange displays a wavelength at maximum absorbance at 464 nm for pH 10 and at 475 nm for pH 4.[53] The absorbance spectra of an aqueous solution of 4 ppm methyl orange at pH 10 and 4 were almost identical for all types of cuvettes, observing the expected shift in the maxima (Figure 5c and Figure S9, Supporting Information). To expand the use of SH cuvettes to other optical measurements, a dispersion of silica nanoparticles was measured by DLS. An important feature of cuvettes for DLS is that they should not scatter light as well as not absorbing light at the wavelength (λ) of the laser, here λ = 660 nm. The average hydrodynamic diameters of the silica nanoparticles measured in the quartz, PS, and self-healing (SH) cuvettes were 30 ± 1, 32 ± 1, and 31 ± 1 nm, respectively (Figure 5d). The polydispersity index (PDI) determined in the quartz, PS, and SH cuvettes were 0.18, 0.21, and 0.18. These DLS and UV–vis experiments showed that the self-healing cuvette can be successfully used for measurements of hydrodynamic diameters and absorbance without loss of accuracy and without limited durability.

In addition to optical measurements, PU-SH elastomers can be used as transparent containers to encapsulate and seal various solid and liquid chemicals. First, a hollow cylinder was filled with an aqueous solution of rhodamine B by injecting with a syringe needle (**Figure 6**a) and subsequently healing the punctured hole. The PU-SH capsule did not show any leakage of the fluorescent dye. Due to its dynamic properties, the shape of the container with the sealed liquid inside can be reconfigured on demand to fit the needs of application. A hollow cylinder filled with an encapsulated rhodamine B aqueous solution was deformed by mechanical compression at temperature of 25 or 70 °C. Whereas the cylindrical shape was recovered after deformation at 25 °C (Figure S10, Supporting Information), the shape was permanently fixed after the heat treatment at 70 °C (Figure 6b). This shows that the PU-SH containers can be deformed either temporarily or permanently (fixing their shape) under mechanical stress without leaking the encapsulated liquid.

To verify the effective sealing of the PU-SH transparent container, sodium hydride was encapsulated in open hollow self-

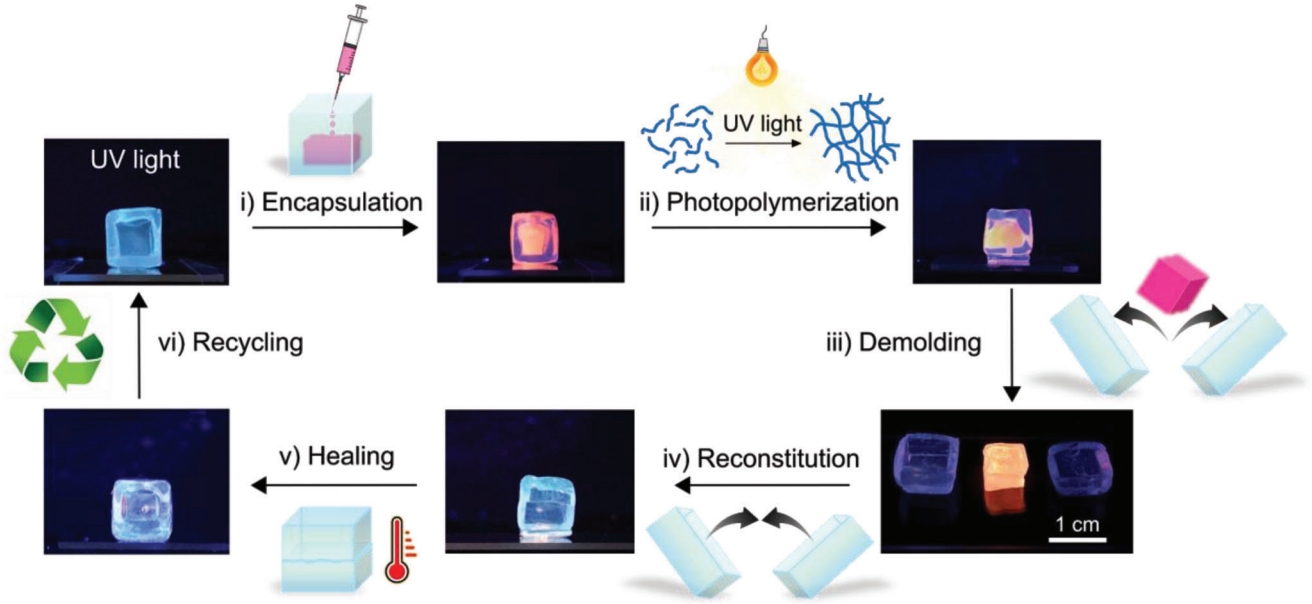

Figure 7. Utilization of a hollow closed cube as reactor for the photopolymerization of trimethylolpropane triacrylate (TMPTA). TMPTA was labeled with Rhodamine B. i) Encapsulation of TMPTA by puncturing the upper face of the cube with a needle (18G), followed by heating at 70 °C for 24 h. ii) Photopolymerization of TMPTA under UV light at a wavelength of 365 nm for 2 min. iii) Demolding by cutting the hollow cube to obtain the cured PTMPTA object. iv) Reconstitution of the cut hollow cube at 25 °C. v) Healing at 70 °C for 24 h to obtain a healed hollow cube. vi) Recycling of the healed hollow cube.

healing cubes, which were sealed by heating, thus taking advantage of the dynamic disulfide bonds of the elastomer (Figure 6c). Sodium hydride was selected as a test material because it reacts violently with water to yield hydrogen gas and sodium hydroxide, and therefore any leakage is easily detected as gas bubbles and a sharp increase in pH. A sealed PU-SH cube containing sodium hydride was immersed in aqueous solutions at pH 5 at 25 °C (Figure 6c,i). After 1.5 h of immersion, the self-healing hollow cube could maintain its shape with intact 3D structure, resulting in a constant pH ≈ 5 without any visible leakage, indicating that the sealing is effective. In parallel, an analogous PU-SH cube containing sodium hydride was punctured and then immersed in a pH 5 aqueous solution (Figure 6c,ii). The formation of bubbles in the surrounding of the cube was immediately observed in the punctured cube (attributed to the formation of hydrogen gas due to reaction with water) and the pH indicator strip turned to different colors of yellow, orange, dark blue, and light yellow, indicating pH ≈ 10 due to the generation of hydroxide ions upon reaction with water. This experiment showed that the sealing of PU-SH 3D objects by healing was efficient and allowed to use them as recipients for protecting chemicals from their environment.

As an example of an encapsulation proof-of-concept application where the self-healing and transparent properties are necessary, we used PU-SH hollow cubes as customizable and recyclable reactor for photopolymerization (**Figure 7**).

Trimethylolpropane triacrylate (TMPTA) was labeled with rhodamine B dye and was encapsulated in the hollow closed PU-SH cube. Then, TMPTA was photopolymerized under UV irradiation. After curing, the PU-SH cube was cut and open and a cube of poly(trimethylolpropane triacrylate) (PTMPTA) could be then demolded and released from the hollow cubic mold. The cut PU-SH molds were then reconstituted and recycled after healing. This demonstration of PU-SH molds, in addition to the fact their shapes can be reconfigured to the desired mold geometry, shows promise in adaptable and recyclable reactors with customizable shapes for flexible 3D fabrication.

3. Conclusions

Transparent polyurethane PU-SH elastomers have been functionalized with self-healing properties through the incorporation of dynamic disulfide bonds in the polymer network. By leveraging these dynamic bonds, 3D polymer structures can be fabricated by folding and modular assembly of 2D flat sheets, followed by a thermal healing process with seam-free joints. The fabricated objects preserve their transparency (92.8% transmittance) and their mechanical stability after multiple cycles of shape-fixing and healing, which enables the customization of 3D structures and their recycling for multiple uses. For these reasons, PU-SH polymers present opportunities as a materials platform for optical devices. We have fabricated PU-SH cuvettes for UV–vis spectroscopy and dynamic light scattering with performance and accuracy equivalent to quartz cuvettes. In addition, PU-SH cuvettes can heal scratch, crack, and abrasion damages in their surface that would typically compromise their function, and thus extend their durability and their lifetime beyond typical limitations. Last, we have explored the use of hollow PU-SH 3D structures as deformable but sealable containers for the encapsulation and protection of chemicals and as reconfigurable and recyclable reactors. We envision that such reconfigurable, transparent, self-healing polymers could be used to design adaptive smart packaging, reconfigurable optical devices, and 3D actuators.

4. Experimental Section

Materials: PTHF ($M_n \approx 1000$ g mol^{-1}, Sigma-Aldrich) was dried at 120 °C under vacuum for 2 h before use. HEDS (≥85.0%, Sigma-Aldrich), HDO (>97.0%, TCI Chemicals), dibutytin dilaurate (DBTDL, 95%, Sigma-Aldrich), HMDI (>90.0%, TCI Chemicals), Rhodamine B (C.I.45170 for microscopy, ≥98.0%, Sigma-Aldrich), sodium hydride (60 wt%, dispersion in paraffin liquid, TCI Chemicals), methyl orange (sodium salt, LabChem Chemicals), TMPTA (>75.0%, TCI Chemicals), methylene blue solution (concentration = 15 g L^{-1}, Sigma-Aldrich), hydrochloric acid (HCl, 37%, Carlo Erba), sodium hydroxide (NaOH, ≥97%, Carlo Erba), Ludox TM-40 colloidal silica (40 wt% suspension in water, Sigma-Aldrich), tetrahydrofuran (THF, ≥99.9%, Carlo Erba), *N*,*N*-dimethylacetamide (DMAc, >99.0%, TCI Chemicals), and nichrome wires (20 wt% chromium in nickel, diameter = 0.2 mm) were used as received. Deionized water was used throughout the experiments. Polyvinyl chloride (PVC) sheets with a thickness of 0.13 mm (Bright office, China) were laminated with a polyester adhesive tape (3 M, USA). The bilayer materials were used for the fabrication of 3D objects, the polyester adhesive tape layer being in contact with the self-healing polyurethane.

Synthesis of Transparent Polyurethanes: PTHF (20.1 g, 20.1 mmol) was first melted in a 250 mL round bottom flask at 70 °C. HMDI (15.2 mL, 62.3 mmol) was then added into the flask and stirred to give a well-mixed mixture, followed by addition of DBTDL (38 µL, 0.06 mmol). After 2 h reaction, a viscous prepolymer solution was obtained and diluted with DMAc (80 mL). The flask was then connected to a digital overhead stirrer (RW 20, IKA) with a polytetrafluoroethylene-coated propeller for stirring the viscous polymer solution. HEDS (5.2 mL, 41.5 mmol) was then charged into the solution and the reaction was allowed to proceed at 70 °C for another 16 h to obtain a self-healing polyurethane (PU-SH). The solution of PU-SH after reaction was diluted with DMAc (55 mL) and THF (20 mL).

A polyurethane without self-healing ability (PU) was prepared following the same aforementioned procedure with the exception that HEDS was replaced by HDO (4.97 g, 42.0 mmol), 45 mL DMAc was used during the reaction (12 h), and that 90 mL DMAc and 20 mL THF were used for diluting the polymer solution after reaction. The apparent weight-average molecular weight (M_w), the apparent number-average molecular weight (M_n), and the molecular weight distribution (MWD) of PU-SH were 77 500 g mol^{-1}, 34 000 g mol^{-1}, and 2.28, respectively. M_w, M_n, and MWD of PU were 119 300 g mol^{-1}, 63 600 g mol^{-1}, and 1.88, respectively.

Fabrication of 3D Objects from 2D Polymer Sheets or 3D Polymer Objects: 2D polymer sheets were prepared by casting the obtained polymer solution in glass petri dishes with a diameter of 150 mm. The films were dried at 60 °C under vacuum for 4 d to obtain polymer sheets with a thickness of 0.78 ± 0.02 mm. Sheets with various 2D shapes were prepared by cutting the circular sheets. Dyed 2D sheets (1.54 mg Rhodamine B g^{-1} polymer or 0.09 mg methylene blue g^{-1} polymer) were prepared followed the same procedure. 2D planar self-healing polymer sheets were then folded into closed hollow cubes (six faces) and open hollow rectangular prisms (five faces), which were covered with PVC hollow cubes and open hollow rectangular prisms to maintain their shapes during heating at 70 °C for 24 h. Similarly, closed hollow cubes (six faces) and closed hollow cylinders (three faces) were prepared by assembling corresponding 2D sheets, which were covered by the corresponding closed hollow PVC scaffolds, followed by heating at 70 °C for 24 h. Closed hollow rectangular prisms (six faces) were obtained by assembling open hollow cubes (five faces), which were covered with open PVC hollow cubes, followed by heating at 70 °C for 24 h.

Photopolymerization inside Self-Healing Hollow Cubes: Photopolymerization of mixture of Rhodamine B in TMPTA (280 mg, 0.3 mg Rhodamine B g^{-1} TMPTA) was carried out with a ultraviolet-visible (UV) light-emitting diode (LED lamp (Awellcure, model 260 × 260, UV intensity = 27.2 mW cm^{-2}) for 6 min at a wavelength of 365 nm. The distance between the lamp and the TMPTA in a hollow cube was 5 cm.

Characterizations for Mechanical and Self-Healing Properties: For healing of scratches on the polymers, the polymer films of PU and PU-SH were cut using a cutter blade to give a scratch (width ≈ 10 µm) on the films, and healed at 70 °C for 30 min. The optical microscopy images were recorded using an optical microscope (IX73, Olympus). Tensile test specimens of PU and PU-SH were prepared as dog-bone shaped specimens with an overall length of 30 mm, a gauge length of 10 mm, a width of 5 mm, and a thickness of 0.2 ± 0.1 mm. The healed specimens were prepared by cutting the pristine films in half using a cutter blade, then the two pieces were put together again and healed at 70 °C in an oven for 24 h. Mechanical tensile tests were performed in triplicates using a texture analyzer (TA.XT Plus, Stable Micro Systems) with a strain rate of 60 mm min^{-1} at 25 °C.

Rheological Measurements: For the investigation on frequency sweep, shape programming of the self-healing polymer was carried out by heating a polymer film (thickness = 0.30 ± 0.02 mm) on a glass substrate at 70 °C for 24 h and subsequently cooling down to 25 °C for 3 h, which was defined as a cycle of shape programming. The polymer film from each cycle was cut into a circular film (diameter ≈ 8 mm) and then subjected to rheological measurements. The rheological properties of polymers were performed using a rheometer (HR30, TA instruments) on a shear mode with a parallel plate (diameter = 8 mm) under a frequency sweep 0.01 to 100 rad s^{-1} between 10 and 90 °C. Specimens were compressed with 1.0 N prior measurements. For the measurements on strain sweep, Circular flat polymer sheets (thickness = 0.78 ± 0.02 mm) were bent along the chord passing the center of the circle (diameter) to an angle of 90°. The bent circular sheets were deposited on two perpendicular glass slides, followed by heating at 70 °C for 24 h. The resulting bent polymer sheet was recovered to the original planar shape by unfolding on glass slides and heating at 70 °C for another 24 h. Three cycles of deformation/recovery of the polymer sheets were carried out. Samples before bending, after each cycle of deformation/recovery was subjected to DMA experiments. DMA were performed in a shear mode at 25 °C using a rheometer (HR20, TA instruments) with a parallel plate (diameter = 20 mm) under a frequency of 0.1 Hz and a dynamic strain sweep of 0.01–100%. Experiments were carried out in triplicates.

Protecting and Sealing Substances in Hollow 3D Self-Healing Containers: Sodium hydride (71.90 mg) was added in open hollow cubes (edge = 8 mm). The cubes were then closed with a square sheet (edge = 8 mm) and heated at 70 °C for 24 h. One intact hollow cube, and one cube which was punctured with a needle (18G) at three difference positions on the upper face of the cube (control sample), were then immersed in 30 mL of a HCl aqueous solution (0.83 M) at 25 °C for 1.5 h. A pH indicator strip (McolorpHast, Merck) was used to monitor the pH value of the aqueous solution after 1.5 h. In another experiment, 0.2 mL of an aqueous solution of Rhodamine B (0.3 mg mL^{-1}) was added in a closed hollow cylinder by puncturing the upper face of the cylinder with a needle (18G), followed by heating at 70 °C for 24 h.

UV–vis Absorption and DLS Measurements with a Self-Healing Cuvette: An open hollow rectangular prism (12.5 mm × 12.5 mm × 45 mm) and a wall's thickness of 0.75 mm was prepared according to the aforementioned procedure applied to the fabrication of 3D objects. The hollow prism was then used as self-healing cuvette.

25 µL of a HCl aqueous solution (0.05 M) or 25 µL of a NaOH aqueous solution (0.05 M) was mixed with 10 mL of a methyl orange aqueous solution (0.004 mg mL^{-1}) to obtain acidic (pH = 4) and basic (pH = 10) methyl orange solutions, respectively. The UV–vis absorbances of the methyl orange aqueous solutions were measured separately with a wavelength range of 340–800 nm in the self-healing cuvette, a quartz cuvette with a pathlength of 10 mm (Hellma analytics), and a polystyrene cuvette with a pathlength of 10 mm (VWR international) at 25 °C. The normalized absorbance of methyl orange aqueous solutions measured in the SH cuvette was divided by 1.1 to take into account the difference of pathlength according to the Beer-Lambert's law. To construct calibration curves, UV–vis absorbances of methylene blue aqueous solutions (0.25, 0.50, 0.75, 1.00, 3.00, and 5.00 ppm) were measured separately in the self-healing and quartz cuvettes. Aqueous solutions of 0.56 and 2.40 ppm methylene blue were then measured separately in the two different cuvettes. Experiments were carried out in triplicates.

Hydrodynamic diameters (D_h) and PDI of 3 mL of a silica dispersion (0.53 wt% in water) were separately measured by DLS with the self-healing, the quartz, and the polystyrene cuvettes at 25 °C. Experiments were carried out in triplicates.

Analytical Methods: The nuclear magnetic resonance (NMR) spectra were recorded with a 600 MHz NMR spectrometer (Avance III HD, Bruker) at 30 °C in THF-d8. Raman spectra of the polymers were collected on a Raman microscope (inVia, Renishaw, UK) under a 20× microscope magnification using a laser excitation wavelength of 532 nm with grating of 1800 lines mm^{-1}. The spectra were recorded between 200 and 1000 cm^{-1} for 10 s of an exposure time at 25 °C. FTIR spectroscopy spectra were recorded using an FTIR spectrometer (Nicolet iS20, Thermo Fisher Scientific) on attenuated total reflectance mode with a wavenumber range of 400–4000 cm^{-1} by 64 scans at a resolution of 4 cm^{-1}. The apparent molecular weights of polymer were measured by gel permeation chromatography (GPC, Viscotek TDAmax, Malvern) with a refractive index detector and three single-pore GPC/size exclusion chromatography columns (6, 7, and 10 µm particle size, linear M). Polymer solutions in THF were filtered through a 0.45 mm pore size polytetrafluoroethylene (PTFE) membrane filter and measured at 35 °C with a flow rate of 1 mL min^{-1}. The system was calibrated with polystyrene standards (Mainz). UV–vis absorption and UV–vis transmittance spectra were recorded with a UV–vis spectrometer (Lambda 1050, PerkinElmer). Baseline correction was carried out with air before measuring UV–vis transmittance of the samples. The hydrodynamic diameter of silica nanoparticles was measured by DLS (NanoPlus, Particulate systems).

For the determination of optical transmittance and haze, rectangular self-healing polymer (1.2 cm × 2.6 cm × 0.78 mm) and polystyrene (1.2 cm × 2.6 cm × 1.0 mm) substrates were subjected to 40 cycles of abrasion with a 1000 grit SiC abrasive paper and followed by healing at 70 °C in an oven for 24 h. The haze values of pristine, abraded, and healed substrates were calculated using the following equation: Haze $(\%) = (\frac{T_4}{T_2} - \frac{T_3}{T_1}) \times 100$ where T_1 is the total incident light, T_2 is the light transmitted by sample, T_3 is the light scattered by instrument, and T_4 is the light scattered by instrument and sample, which were averaged over a visible wavelength range of 380–780 nm. The abrasion–healing cycles were performed in duplicates.

Supporting Information

Supporting Information is available from the Wiley Online Library or from the author.

Acknowledgements

The authors would like to thank Jenpob Sokjorhor at the Vidyasirimedhi Institute of Science and Technology (VISTEC) for his help in NMR measurements. D.C. acknowledges the NSRF, Program Management Unit for Human Resources & Institutional Development (PMU-B, grant B05F640208).

Conflict of Interest

The authors declare no conflict of interest.

Data Availability Statement

The data that support the findings of this study are available from the corresponding author upon reasonable request.

Keywords

elastomers, optical materials, polyurethane, self-healing, shape-programming polymers

Received: June 21, 2022
Revised: August 9, 2022
Published online: September 1, 2022

[1] L. Zhou, X.-X. Dong, G.-C. Lv, J. Chen, S. Shen, *Opt. Commun.* **2015**, *342*, 167.
[2] A. Gadisa, K. Tvingstedt, S. Admassie, L. Lindell, X. Crispin, M. R. Andersson, W. R. Salaneck, O. Inganäs, *Synth. Met.* **2006**, *156*, 1102.
[3] C.-C. Chen, L. Dou, R. Zhu, C.-H. Chung, T.-B. Song, Y. B. Zheng, S. Hawks, G. Li, P. S. Weiss, Y. Yang, *ACS Nano* **2012**, *6*, 7185.
[4] N. Cui, Y. Song, C.-H. Tan, K. Zhang, X. Yang, S. Dong, B. Xie, F. Huang, *npj Flexible Electron.* **2021**, *5*, 31.
[5] L. Han, L. Yan, M. Wang, K. Wang, L. Fang, J. Zhou, J. Fang, F. Ren, X. Lu, *Chem. Mater.* **2018**, *30*, 5561.
[6] J. Kim, J. Park, Y.-G. Park, E. Cha, M. Ku, H. S. An, K.-P. Lee, M.-I. Huh, J. Kim, T.-S. Kim, D. W. Kim, H. K. Kim, J.-U. Park, *Nat. Biomed. Eng.* **2021**, *5*, 772.
[7] P. Won, K. K. Kim, H. Kim, J. J. Park, I. Ha, J. Shin, J. Jung, H. Cho, J. Kwon, H. Lee, S. H. Ko, *Adv. Mater.* **2021**, *33*, 2002397.
[8] P. Li, Y. Wang, U. Gupta, J. Liu, L. Zhang, D. Du, C. C. Foo, J. Ouyang, J. Zhu, *Adv. Funct. Mater.* **2019**, *29*, 1901908.
[9] H. Yuk, S. Lin, C. Ma, M. Takaffoli, N. X. Fang, X. Zhao, *Nat. Commun.* **2017**, *8*, 14230.
[10] H. Wu, Q. Liu, W. Du, C. Li, G. Shi, *ACS Appl. Mater. Interfaces* **2018**, *10*, 3895.
[11] Z.-H. Jin, Y.-L. Liu, J.-J. Chen, S.-L. Cai, J.-Q. Xu, W.- H. Huang, *Anal. Chem.* **2017**, *89*, 2032.
[12] J. Kang, D. Son, G.-J. N. Wang, Y. Liu, J. Lopez, Y. Kim, J. Y. Oh, T. Katsumata, J. Mun, Y. Lee, L. Jin, J. B.-H. Tok, Z. Bao, *Adv. Mater.* **2018**, *30*, 1706846.
[13] Y. Cao, H. Wu, S. I. Allec, B. M. Wong, D.-S. Nguyen, C. Wang, *Adv. Mater.* **2018**, *30*, 1804602.
[14] Y. He, S. Liao, H. Jia, Y. Cao, Z. Wang, Y. Wang, *Adv. Mater.* **2015**, *27*, 4622.
[15] J. Li, J. Liang, L. Li, F. Ren, W. Hu, J. Li, S. Qi, Q. Pei, *ACS Nano* **2014**, *8*, 12874.
[16] A. J. Bandodkar, C. S. López, A. M. Vinu Mohan, L. Yin, R. Kumar, J. Wang, *Sci. Adv.* **2016**, *2*, e1601465.
[17] A. Pena-Francesch, H. Jung, M. C. Demirel, M. Sitti, *Nat. Mater.* **2020**, *19*, 1230.
[18] S. Terryn, J. Brancart, D. Lefeber, G. Van Assche, B. Vanderborght, *Sci. Rob.* **2017**, *2*, eaan4268.
[19] S. Wang, M. W. Urban, *Nat. Rev. Mater.* **2020**, *5*, 562.
[20] Y. Yang, M. W. Urban, *Chem. Soc. Rev.* **2013**, *42*, 7446.
[21] M. D. Hager, P. Greil, C. Leyens, S. Van Der Zwaag, U. S. Schubert, U. S. Schubert, *Adv. Mater.* **2010**, *22*, 5424.
[22] R. Martin, A. Rekondo, A. Ruiz De Luzuriaga, G. Cabañero, H. J. Grande, I. Odriozola, *J. Mater. Chem. A* **2014**, *2*, 5710.
[23] H. Zhang, D. Wang, N. Wu, C. Li, C. Zhu, N. Zhao, J. Xu, *ACS Appl. Mater. Interfaces* **2020**, *12*, 9833.
[24] Z. Wang, Y. Gu, M. Ma, M. Chen, *Macromolecules* **2020**, *53*, 956.
[25] Z. Fang, N. Zheng, Q. Zhao, T. Xie, *ACS Appl. Mater. Interfaces* **2017**, *9*, 22077.
[26] J. Lou, Z. Liu, L. Yang, Y. Guo, D. Lei, Z. You, *Adv. Funct. Mater.* **2021**, *31*, 2008328.
[27] Y. Yang, E. M. Terentjev, Y. Wei, Y. Ji, *Nat. Commun.* **2018**, *9*, 1906.
[28] X. Qiu, Q. Guo, Y. Wang, X. Huang, J. Cao, Z. Zheng, X. Zhang, *ACS Appl. Mater. Interfaces* **2020**, *12*, 41981.
[29] Y. Bai, J. Zhang, D. Wen, P. Gong, J. Liu, J. Ju, X. Chen, *Compos. Sci. Technol.* **2020**, *187*, 107940.
[30] D. H. Gracias, J. Tien, T. L. Breen, C. Hsu, G. M. Whitesides, *Science* **2000**, *289*, 1170.
[31] R. V. Martinez, C. R. Fish, X. Chen, G. M. Whitesides, *Adv. Funct. Mater.* **2012**, *22*, 1376.
[32] T. G. Leong, B. R. Benson, E. K. Call, D. H. Gracias, *Small* **2008**, *4*, 1605.
[33] N. Turner, B. Goodwine, M. Sen, *Proc. Inst. Mech. Eng., Part C* **2016**, *230*, 2345.

[34] S. Felton, M. Tolley, E. Demaine, D. Rus, R. Wood, *Science* **2014**, *345*, 644.
[35] C. L. Randall, E. Gultepe, D. H. Gracias, *Trends Biotechnol.* **2012**, *30*, 138.
[36] A. Kirillova, L. Ionov, *J. Mater. Chem. B* **2019**, *7*, 1597.
[37] R. Fernandes, D. H. Gracias, *Adv. Drug Delivery Rev.* **2012**, *64*, 1579.
[38] S.-M. Kim, H. Jeon, S.-H. Shin, S.-A. Park, J. Jegal, S. Y. Hwang, D. X. Oh, J. Park, *Adv. Mater.* **2018**, *30*, 1705145.
[39] A. Rekondo, R. Martin, A. Ruiz de Luzuriaga, G. Cabañero, H. J. Grande, I. Odriozola, *Mater. Horiz.* **2014**, *1*, 237.
[40] H. Guo, Y. Han, W. Zhao, J. Yang, L. Zhang, *Nat. Commun.* **2020**, *11*, 2037.
[41] Y. Lai, X. Kuang, P. Zhu, M. Huang, X. Dong, D. Wang, *Adv. Mater.* **2018**, *30*, 1802556.
[42] X. Wang, H. Zhang, B. Yang, L. Wang, H. Sun, *New J. Chem.* **2020**, *44*, 5746.
[43] T. Li, T. Zheng, J. Han, Z. Liu, Z.-X. Guo, Z. Zhuang, J. Xu, B.-H. Guo, *Polymers* **2019**, *11*, 838.
[44] X. Li, R. Yu, Y. He, Y. Zhang, X. Yang, X. Zhao, W. Huang, *ACS Macro Lett.* **2019**, *8*, 1511.
[45] C. C. Hornat, M. W. Urban, *Nat. Commun.* **2020**, *11*, 1028.
[46] S. Zechel, R. Geitner, M. Abend, M. Siegmann, M. Enke, N. Kuhl, M. Klein, J. Vitz, S. Gräfe, B. Dietzek, M. Schmitt, J. Popp, U. S. Schubert, M. D. Hager, *NPG Asia Mater.* **2017**, *9*, e420.
[47] J. He, F. Song, X. Li, L. Chen, X. Gong, W. Tu, *J. Polym. Res.* **2021**, *28*, 122.
[48] X. Song, X. Zhang, T. Li, Z. Li, H. Chi, *Polymers* **2019**, *11*, 373.
[49] A. Farzaneh, A. Rostami, H. Nazockdast, *Polym. Compos.* **2021**, *42*, 4804.
[50] Z. S. Khalifa, *RSC Adv.* **2017**, *7*, 30295.
[51] J. Lindahl, J. T. Wätjen, A. Hultqvist, T. Ericson, M. Edoff, T. Törndahl, *Prog. Photovoltaics: Res. Appl.* **2013**, *21*, 1588.
[52] K.-C. Peng, H.-C. Kao, S.-J. Liu, K.-L. Tsai, J.-C. Lin, *Jpn. J. Appl. Phys.* **2013**, *52*, 11NB04.
[53] J. Del Nero, R. E. De Araujo, A. S. L. Gomes, C. P. De Melo, *J. Chem. Phys.* **2005**, *122*, 104506.